Lithium-Ion Batteries

International Edition: DOI: 10.1002/anie.201410807
German Edition: DOI: 10.1002/ange.201410807

Self-Sustained Cycle of Hydrolysis and Etching at Solution/Solid Interfaces: A General Strategy To Prepare Metal Oxide Micro-/Nanostructured Arrays for High-Performance Electrodes**

Yingmeng Zhang, Weixin Zhang, Zeheng Yang, Heyun Gu, Qing Zhu, Shihe Yang,* and Mei Li*

Abstract: *Assembling micro-/nanostructured arrays on conducting substrates allows the integration of multiple functionalities into modern electronic devices. Herein, a novel self-sustained cycle of hydrolysis and etching (SCHE) is exploited to selectively synthesize an extensive series of metal oxide micro-/nanostructured arrays on a wide range of metal substrates, establishing the generality and efficacy of the strategy. To demonstrate the potential application of this method, the as-prepared NiO porous nanobelt array was directly used as the anode for lithium-ion batteries, exhibiting excellent capacity and rate capability. Conclusively, the SCHE strategy offers a systematic approach to design metal oxide micro-/nanostructured arrays on metal substrates, which are valuable not only for lithium-ion batteries but also for other energy conversion and storage systems and electronic devices at large.*

Metal oxides are fascinating functional materials and have been widely exploited in various technological fields.[1–6] To meet the ever-growing demand for high-performance devices, it is highly desirable to grow self-supported metal oxide micro-/nanostructured arrays on conducting substrates as electrodes directly. The integration of hierarchical micro-/nanostructures with well-ordered arrays on conducting substrates facilitates the synergy and incorporation of multiple functionalities into modern electronic devices, such as lithium-ion batteries (LIBs),[1] supercapacitors (SCs),[2] and solar cells,[3] as well as electrochromic devices[4] and light-emitting diodes.[5] The hierarchical micro-/nanostructures have abundant electrode/electrolyte interfaces and decrease diffusion distance to the interior surface, leading to kinetic acceleration of the electrochemical reactions.[6] Moreover, the well-ordered arrays closely connected to the current collectors can provide direct electron-transport pathways, leading to enhanced performances of the electronic devices.[1–5] Additionally, the in situ growth of active materials on the conducting substrates greatly simplifies the electrode fabrication process without requiring the use of any binders or conductive additives.[1–5]

Fabrication of micro-/nanostructured arrays of metal oxides or their precursors on metal substrates is often based on the following two strategies. The first strategy involves in situ growth on the metal substrates, such as direct thermal oxidation,[7] electrochemical anodization,[8] and solution-based oxidation.[9] The substrates not only take part in the reactions by chemical oxidation and act as a source of metallic ions, but also serve as a support for the array–film formation. For example, we have developed an aqueous bulk solution or a confined microemulsion reaction for preparing $Cu(OH)_2$ nanorods or hierarchical microcog arrays on Cu substrates, with alkaline $(NH_4)_2S_2O_8$ as oxidant.[9] However, in this case only metal oxides or precursors with the same metal elements as the metal substrates can be obtained. In the other case, the metal substrates act merely as a support and template for the material deposition and are not involved in the chemical reactions, such as in chemical vapor deposition (CVD),[10] chemical bath deposition (CBD),[11] and hydrothermal deposition.[12] For instance, Fan et al. adopted a hydrothermal method to grow CoO nanorod arrays on nickel foams with $Co(NO_3)_2$ as the cobalt source.[12a] The deposition usually takes place not only on the substrates, but also randomly on inside surfaces of the vessel.

Herein, we report a general approach that unifies the in situ synthesis of single or binary component micro-/nanostructured array films of metal oxides or their precursors on metal substrates such as Ni, Co, Zn, Cd, Ti, and Al. This strategy is based on a mechanism involving a self-sustained cycle of hydrolysis and etching (SCHE) occurring at the interfaces between acidic solutions and metal substrates. This method provides a simple and convenient route to assemble a variety of ordered building blocks on metal substrates (current collectors) with novel micro-/nanostructures and synergetic functions as electrodes for different electronic devices.

We chose NiO as an example to demonstrate the effectiveness of this method in yielding micro-/nanostructured arrays on a Ni substrate as an electrode for LIBs. Scheme 1 shows the self-sustained cycle of hydrolysis and etching (SCHE) employed to synthesize $Ni(SO_4)_{0.3}(OH)_{1.4}$

[*] Y. M. Zhang, Prof. Dr. W. X. Zhang, Prof. Dr. Z. H. Yang, H. Y. Gu, Q. Zhu
School of Chemistry and Chemical Engineering
Hefei University of Technology
Hefei, Anhui 230009 (P. R. China)
E-mail: wxzhang@hfut.edu.cn
Prof. Dr. S. H. Yang
Department of Chemistry
William Mong Institute of Nano Science and Technology
The Hong Kong University of Science and Technology
Clear Water Bay, Kowloon, Hong Kong (P. R. China)
E-mail: chsyang@ust.hk
Dr. M. Li
School of Chemistry, Centre for Organized Matter Chemistry
University of Bristol, Bristol BS8 1TS (UK)

[**] We are grateful for the financial support of the National Natural Science Foundation of China (NSFC Grant 21271058).

Supporting information for this article is available on the WWW under http://dx.doi.org/10.1002/anie.201410807.

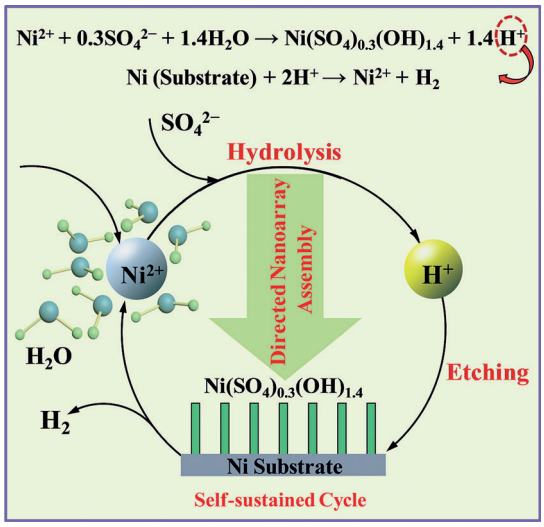

Scheme 1. The self-sustained cycle of hydrolysis and etching (SCHE) can be used to form $Ni(SO_4)_{0.3}(OH)_{1.4}$ nanobelt arrays on a nickel substrate, which is itself a participant of the cycle.

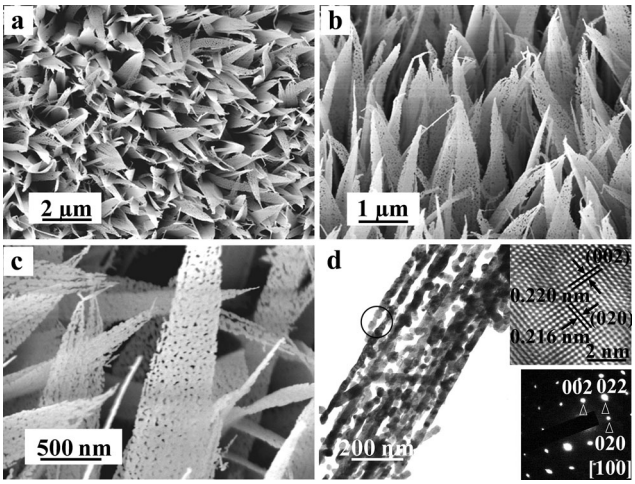

Figure 1. a, b, c) FESEM images of the free-standing NiO porous nanobelt arrays; d) TEM image of an individual porous NiO nanobelt. Insets in (d): HRTEM image in the circled region on a NiO nanobelt (top) and an SAED pattern (bottom).

nanobelt arrays. The reaction system comprises a Ni substrate and a $Ni(NO_3)_2$–Na_2SO_4 aqueous solution, and is subjected to hydrothermal treatment at 160 °C for 12 h with no use of alkali precipitants. When external Ni^{2+} ions in the aqueous solution started to hydrolyze under hydrothermal conditions, hydrolysis products and H^+ ions were generated correspondingly.[13] The H^+ ions were then consumed by etching the nickel substrate to produce Ni^{2+} ions and H_2, which in turn accelerated the hydrolysis of Ni^{2+} ions in an autocatalytic fashion, leading to a preferential hydrolysis on the surface of the nickel substrate. As the reaction continued, the Ni^{2+} ions released from the Ni substrate supplemented the starting Ni^{2+} ions in the solution, establishing a self-sustained cycle of hydrolysis, etching, and deposition occurring near and on the substrate surface. Finally, the NiO film composed of a porous nanobelt array could be obtained by post-heat treatment of the $Ni(SO_4)_{0.3}(OH)_{1.4}$ precursor film.

The X-ray diffraction (XRD) pattern (see Figure S1 in Supporting Information) presents the structural evolution from monoclinic $Ni(SO_4)_{0.3}(OH)_{1.4}$ to cubic NiO through a subsequent post-heat treatment. Figure 1 shows the field-emission scanning electron microscopy (FESEM) and transmission electron microscopy (TEM) images of NiO nanobelt arrays aligned on the nickel substrate. The NiO nanobelt structures have lengths of several μm and widths of 300–600 nm (Figure 1 a, b). These images show that the belt-like architecture of the $Ni(SO_4)_{0.3}(OH)_{1.4}$ precursor (Figure S2) has been preserved after post-heating at 600 °C for 2 h under a nitrogen atmosphere. A close examination reveals that the nanobelts contain numerous nanopores (Figure 1 c), distinct from the continuous structure of the $Ni(SO_4)_{0.3}(OH)_{1.4}$ nanobelts. Clearly, these porous structures result from the transition of $Ni(SO_4)_{0.3}(OH)_{1.4}$ into NiO during the post-heating process. The TEM image in Figure 1 d further confirms the porous structure of each individual NiO nanobelt, which in fact consists of rod-like assemblies of nanoparticles. The lower inset image in Figure 1 d shows the corresponding selected-area electron diffraction (SAED) pattern, which can be indexed to the [100] zone axis of the NiO nanobelt grown parallel to [011]. The HRTEM image (upper inset image in Figure 1 d) of the subunit shows that the marked lattice fringe spacings of 0.216 and 0.220 nm correspond to those of (020) and (002) planes of cubic NiO, respectively. NiO nanobelts with porous structure have a higher BET surface area of 36.6 $m^2 g^{-1}$ than 26.9 $m^2 g^{-1}$ for the precursor $Ni(SO_4)_{0.3}(OH)_{1.4}$ (Figure S3).

The ordered $Ni(SO_4)_{0.3}(OH)_{1.4}$ nanoarray film was selectively grown on the surface of the substrate without random deposition on the inside surfaces of the Teflon-lined wall (Figure S4a,b) under selected conditions. However, when the H^+ ions were overly consumed by OH^- ions coming from the hydrolysis of anions such as acetate ions or from an alkaline reagent such as triethanolamine, no well-defined film could be obtained. Instead, precipitates in powder form were formed in the solution (Figure S4c,d), or on the inside surfaces of the Teflon-lined wall as well as on the substrate (Figure S4e–h). Control experiments showed that without the nickel substrate or with inert substrates, such as glass or Si wafer, there was no deposition in the reactor when hydrothermally treated at 140–180 °C for 24 h. The pH-dependent studies further showed that the reaction system containing the Ni substrate always exhibited a higher pH value than the one with a Si wafer substrate as a result of the consumption of H^+ ions by etching of the Ni substrate (Figure S5). On the other hand, the hydrothermal temperature is also a key factor for activating the hydrolysis reaction and etching the substrate during preparation of the $Ni(SO_4)_{0.3}(OH)_{1.4}$ precursor, as an obvious film on the substrate is obtained only above 140 °C. It should be pointed out that different reaction systems will definitely have different temperature windows for the array synthesis because of the different hydrolytic capacities.

In a broad sense, when the appropriate amount of external metal ions added was hydrolyzed in an aqueous solution, the alkaline-based precursor films were formed on the substrate,

and the produced H^+ ions then made the solution acidic. At the same time, the metal substrates were gradually etched by H^+ ions from the hydrolysis, which in turn promoted the hydrolysis by consuming the H^+ ions, leading to the oriented deposition of alkaline-based precursors on the substrates. Meanwhile, the metal ions released from the metal substrates supplement the consumed metal ions in this hydrolysis system, building up a self-sustained cycle of hydrolysis and etching. As a result, the SCHE strategy allows substrate-specific deposition without random precipitation because the consumption of H^+ ions leads to a preferential hydrolysis on the metal substrate surface. The collateral assembly of the micro-/nanostructured array films on the metal substrates can prevent the metals from being further etched in the acidic solution.

The SCHE method for the formation of $Ni(SO_4)_{0.3}(OH)_{1.4}$ nanobelt arrays can be easily extended to other metal substrates. This can be achieved by replacing the Ni substrate with other metal substrates which can also be etched using a similar system (Figure S6).

By tuning the parameters of the cycle, including the reagents and metal substrates, we are able to prepare different types of metal-based micro-/nanostructured arrays on various substrates. Figure 2 shows several examples of this strategy. Figure 2a shows the Mn-based amorphous nanosheet arrays grown on Ni substrates (Figure S7). $Fe(OH)_3$ nanosheet arrays composed of interconnected nanoflakes have been grown on Ni substrates (Figure 2b; Figure S8). TiO_2 nanorod arrays have also been prepared on a Ti substrate (Figure 2c; Figure S9) with each hierarchical TiO_2 nanorod assembled by nanofilament substructures. AlOOH nanosheet arrays have been grown on an Al substrate and are composed of many cluster subunits which self-assembled through interactions between parts of nanosheets (Figure 2d; Figure S10). $Co(OH)_2$ nanoplate arrays, consisting of a large number of nanoplatelets crosslinked with each other, are vertically aligned on a Co substrate (Figure 2e, Figure S11). Figure 2f shows the composite $Ni(OH)_2$/ZnO nanosheet array film grown on a Zn substrate with crosslinked nanosheets (Figure S12a–c). The corresponding metal oxides (Figure S13), including binary metal oxides (Figure S13c–f), can be derived from thermal treatment of these precursors.

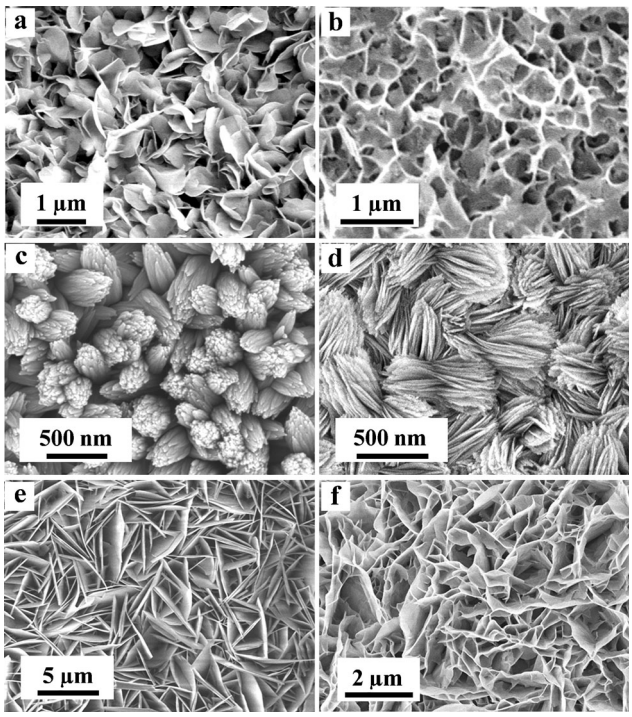

Figure 2. FESEM images of a) Mn-based (amorphous) and b) $Fe(OH)_3$ nanosheet arrays grown on Ni substrates, c) TiO_2 nanorod arrays grown on a Ti substrate, d) AlOOH nanosheet arrays grown on an Al substrate, e) $Co(OH)_2$ nanoplate arrays grown on a Co substrate, and f) $Ni(OH)_2$/ZnO composite nanosheet arrays grown on a Zn substrate.

In the designed reaction systems, the metal ions involved in the hydrolysis reaction come from two sources: the first is an external supply added before the reaction and the second is derived from etching substrates. The two sources can be the same type of metal ion or can be different from each other. In the case when the metal ions derived from etching substrates are different from the external supply, the resultant metal-based micro-/nanostructured arrays were dependent on the solubility product constant (K_{sp}) values of both metallic compounds (Table S1). For example, if one K_{sp} value is much smaller than the other one, then only a single component is expected. For example, the K_{sp} value of $Fe(OH)_3$ (2.64×10^{-39}) is much smaller than that of $Ni(OH)_2$ (5.47×10^{-16}). As a result, only $Fe(OH)_3$ nanowall arrays are obtained on a Ni substrate when nickel foam is immersed in a $Fe(NO_3)_3$ solution (Figure 2b). On the other hand, if both sources meet the hydrolysis condition and exceed their K_{sp} value, then binary metal-based composites can be obtained. For example, the K_{sp} values of $Co(OH)_2$ (5.92×10^{-15}) and $Cd(OH)_2$ (5.27×10^{-15}) are very close, so $Co(OH)_2$/$Cd(OH)_2$ a composite nanoplate-array film is obtained on a Cd substrate (Figure S12d–f), similar to the $Ni(OH)_2$/ZnO nanosheet arrays grown on a Zn substrate (Figure 2f; Figure S12a–c). This method provides a new route for designing micro-/nanostructured array films on metal substrates and enables the fabrication of well-oriented arrays without the use of any templates. More importantly for application of the system, the fabrication can be easily achieved on a large-area substrate ($\geq 40\ cm^2$; Figure S14).

To demonstrate the use of the well-ordered arrays, the as-prepared NiO porous nanobelt-array films (NiO-PNAFs) on a Ni substrate were directly used as anode electrodes for LIBs. The initial ten discharge–charge curves of the NiO-PNAF electrode recorded at a rate of 0.1 C are shown in Figure 3a. The initial discharge capacity is $1017\ mA\,h\,g^{-1}$ with a charge capacity of $737\ mA\,h\,g^{-1}$ and the second discharge capacity is $815\ mA\,h\,g^{-1}$. The potential plateaus and reproducibility of the discharge–charge profiles are in good agreement with the results obtained from the cyclic voltammograms (CV; Figure 3b). A broad cathodic wave centered at 1.18 V and a sharp anodic wave at 1.97 V are identified in the first cyclic voltammogram. After the electrode activation of the first cycle, a set of sharp waves at 1.34 and 1.97 V can be detected during the subsequent cycles. The separations

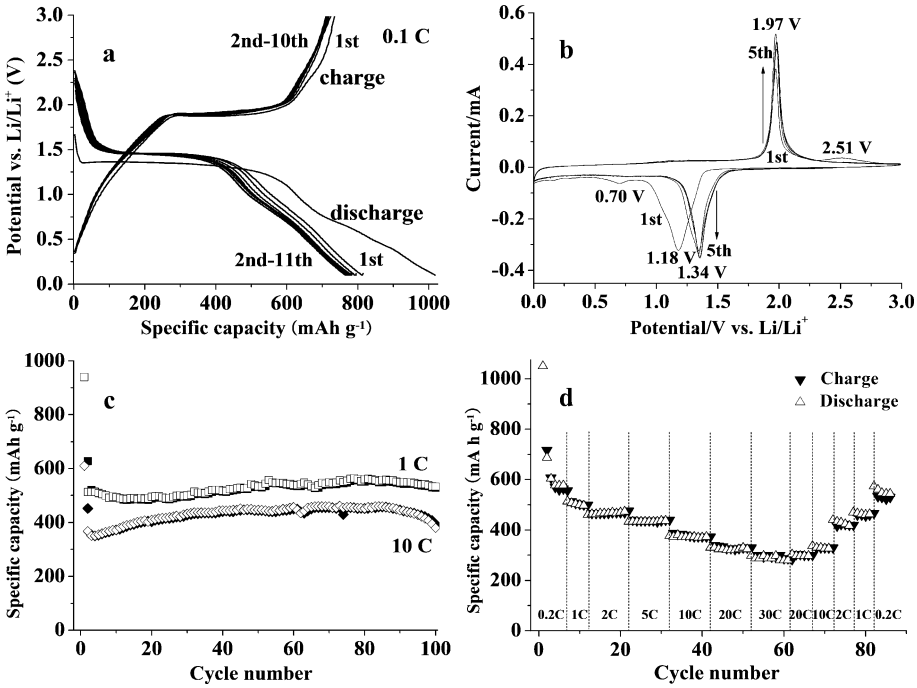

Figure 3. Electrochemical performance of the porous NiO nanobelt-array films as a LIB anode on a Ni substrate (voltage range 0.1–3 V): a) Selected discharge–charge profiles (0.1 C), b) cyclic voltammograms at a scan rate of 0.1 $mV s^{-1}$, c) cycling performance at current densities of 1 C and 10 C, and d) rate cyclability at various rates (1 C = 718 $mA g^{-1}$).

between discharge–charge plateaus and between CV cathodic and anodic waves are much smaller than in previous reports,[9,11a] which indicates the weaker polarization of the NiO-PNAF electrode, and further implies the fast electrochemical reaction kinetics.

The cycling performance of the NiO-PNAF electrodes at current densities of 1 C and 10 C is shown in Figure 3c. It can be seen that the specific capacities increase to a maximum value and then start to decrease, leading to high capacity retentions for 100 cycles. This increase might be attributed to a reversible formation of the gel-like polymer layer.[14] The stable capacity retention at such high current densities indicates its excellent cycling stability and good rate capability. Figure 3d further confirms that the NiO film electrode with 1D porous nanobelt arrays exhibits good rate performance. It delivers average capacities of 440, 380, 330, and 290 $mA h g^{-1}$ at current densities of 5, 10, 20, and 30 C, respectively. When the rate decreased from 30 C down to 0.2 C, the reversible capacity recovers back to 560 $mA h g^{-1}$.

The self-supported arrays directly constructed on the current collector facilitate the efficient diffusion of electrolyte into the inner region of the electrode and sustain the volume change associated with lithium lithiation and delithiation. Additionally, the nanobelt arrays have direct 1D electronic pathways allowing for faster electron transport and the thinness of the nanobelts shortens the pathway of ion transport. Furthermore, micro-/nanoarchitectures which have some surfaces and interfaces fused together have relatively smaller specific surface area than nanostructures, which could lessen the formation of excessive solid–electrolyte interfaces (SEI).

In conclusion, we have demonstrated a new and versatile strategy involving a self-sustained cycle of hydrolysis and etching (SCHE) to directly fabricate a series of metal-based micro-/nanostructured array films on various metal substrates. This method is simple, efficient, and green. In contrast to conventional methods, the synthesis is conducted in non-alkaline aqueous solutions without additional oxidants and alkali reagents. The self-sustained cycle allows substrate-specific deposition instead of random deposition. This general method can be employed to produce a variety of single- or binary-component arrays (employing Ti-, Al-, Ni-, Co-, Mn-, Fe-, Zn-, or Cd-based precursors/oxides) on various functional substrates (such as Ti, Al, Ni, Co, Zn, and Cd foils) by tuning the cycle parameters and is expected to be applicable for large-scale preparation. These arrays of metal oxides grown on functional substrates are anticipated to be applied as promising electrodes not only in lithium-ion batteries, but also in other energy conversion and storage systems, and more broadly in electronic devices wherein micro-/nanostructured arrays are desirable.

Keywords: electrochemistry · energy conversion · hydrolysis · lithium-ion batteries · metal oxides

How to cite: *Angew. Chem. Int. Ed.* **2015**, *54*, 3932–3936
Angew. Chem. **2015**, *127*, 4004–4008

[1] a) B. L. Ellis, P. Knauth, T. Djenizian, *Adv. Mater.* **2014**, *26*, 3368; b) Y. G. Li, B. Tan, Y. Y. Wu, *Nano Lett.* **2008**, *8*, 265; c) P. L. Taberna, S. Mitra, P. Poizot, P. Simon, J. M. Tarascon, *Nat. Mater.* **2006**, *5*, 567.

[2] a) J. Jiang, Y. Y. Li, J. P. Liu, X. T. Huang, C. Z. Yuan, X. W. Lou, *Adv. Mater.* **2012**, *24*, 5166; b) Q. Li, Z. L. Wang, G. R. Li, R. Guo, L. X. Ding, Y. X. Tong, *Nano Lett.* **2012**, *12*, 3803.

[3] M. Law, L. E. Greene, J. C. Johnson, R. Saykally, P. D. Yang, *Nat. Mater.* **2005**, *4*, 455.

[4] a) R. S. Devan, S. Y. Gao, W. D. Ho, J. H. Lin, Y.-R. Ma, P. S. Patil, Y. Liou, *Appl. Phys. Lett.* **2011**, *98*, 133117; b) A. Ghicov, S. P. Alba, J. M. Macak, P. Schmuki, *Small* **2008**, *4*, 1063.

[5] a) R. S. Devan, R. A. Patil, J. H. Lin, Y.-R. Ma, *Adv. Funct. Mater.* **2012**, *22*, 3326; b) S. Xu, C. Xu, Y. Liu, Y. F. Hu, R. S. Yang, Q. Yang, J. H. Ryou, H. J. Kim, Z. Lochner, S. Choi, R. Dupuis, Z. L. Wang, *Adv. Mater.* **2010**, *22*, 4749.

[6] a) C. Yuan, H. B. Wu, Y. Xie, X. W. Lou, *Angew. Chem. Int. Ed.* **2014**, *53*, 1488; *Angew. Chem.* **2014**, *126*, 1512; b) Q. F. Zhang, E. Uchaker, S. L. Candelaria, G. Z. Cao, *Chem. Soc. Rev.* **2013**, *42*, 3127.

[7] a) X. G. Wen, S. H. Wang, Y. Ding, Z. L. Wang, S. H. Yang, *J. Phys. Chem. B* **2005**, *109*, 215; b) C. H. Xu, C. H. Woo, S. Q. Shi, *Chem. Phys. Lett.* **2004**, *399*, 62.

[8] a) J. H. Kim, K. Zhu, Y. F. Yan, C. L. Perkins, A. J. Frank, *Nano Lett.* **2010**, *10*, 4099; b) S. K. Mohapatra, S. E. John, S. Banerjee, M. Misra, *Chem. Mater.* **2009**, *21*, 3048.
[9] a) Y. M. Zhang, W. X. Zhang, M. Li, Z. H. Yang, G. D. Chen, Q. Wang, *J. Mater. Chem. A* **2013**, *1*, 14368; b) W. X. Zhang, M. Li, Q. Wang, G. D. Chen, M. Kong, Z. H. Yang, S. Mann, *Adv. Funct. Mater.* **2011**, *21*, 3516; c) W. X. Zhang, S. H. Yang, *Acc. Chem. Res.* **2009**, *42*, 1617.
[10] a) B. Xiang, P. Wang, X. Zhang, S. A. Dayeh, D. P. R. Aplin, C. Soci, D. Yu, D. Wang, *Nano Lett.* **2007**, *7*, 323; b) G. Malandrino, S. T. Finocchiaro, R. Lo Nigro, C. Bongiorno, C. Spinella, I. L. Fragalà, *Chem. Mater.* **2004**, *16*, 5559.
[11] a) X. H. Huang, J. P. Tu, X. H. Xia, X. L. Wang, J. Y. Xiang, L. Zhang, Y. Zhou, *J. Power Sources* **2009**, *188*, 588; b) S.-Y. Han, D.-H. Lee, Y.-J. Chang, S.-O. Ryu, T.-J. Lee, C.-H. Chang, *J. Electrochem. Soc.* **2006**, *153*, C382.
[12] a) C. Guan, X. H. Xia, N. Meng, Z. Y. Zeng, X. H. Cao, C. Soci, H. Zhang, H. J. Fan, *Energy Environ. Sci.* **2012**, *5*, 9085; b) J. P. Liu, J. Jiang, C. W. Cheng, H. X. Li, J. X. Zhang, H. Gong, H. J. Fan, *Adv. Mater.* **2011**, *23*, 2076.
[13] a) J. P. Liu, Y. Y. Li, H. J. Fan, Z. H. Zhu, J. Jiang, R. M. Ding, Y. Y. Hu, X. T. Huang, *Chem. Mater.* **2010**, *22*, 212; b) M. S. Wu, K. C. Huang, *Chem. Commun.* **2011**, *47*, 12122.
[14] a) Y. Wu, Y. Wei, J. P. Wang, K. L. Jiang, S. S. Fan, *Nano Lett.* **2013**, *13*, 818; b) S. Laruelle, S. Grugeon, P. Poizot, M. Dollé, L. Dupont, J.-M. Tarascon, *J. Electrochem. Soc.* **2002**, *149*, A627.

Received: November 6, 2014
Revised: January 8, 2015
Published online: February 4, 2015

